CTES, L.P.
9870 Pozos Lane
Conroe, Texas 77303
phone: (936) 521-2200
fax: (936) 5221-2275
www.ctes.com

Achilles 4.0
CT Fatigue Life Prediction Algorithm

Subject Matter Authority: Steven M. Tipton, Ph.D., P.E., The University of Tulsa

May 21, 2003

Contents

Introduction

A coiled tubing fatigue life prediction algorithm was delivered to CTES in March, 2003, referred to as TFATIGUE. This DLL serves as the engine used by Achilles 4.0 for making fatigue life predictions. A previous version, referred to as YFATIGUE, Version 3.3, was the life prediction module used by Achilles 3.0.

This document describes rationale behind the development of TFATIGUE and documents its differences with YFATIGUE, which will be referred to as V4 and V3 respectively, for the remainder of this document (for version 4.0 and 3.0 of Achilles, respectively.) Since the two algorithms share the same basic life estimation philosophy, this document does not reproduce details contained in Reference 1.

Both V3 and V4 make CT life predictions as follows: The fluctuation in the state of stress and strain caused by a bending or straightening event is computed using an incremental plasticity algorithm. The change in equivalent strain is used with the prevailing internal pressure to compute "effective strain amplitude." The effective strain amplitude is used to enter a strain-life curve to predict fatigue damage associated with that event. The damage is summed linearly, but can accrue at a nonlinear rate, since the equivalent strain increases during loading at high internal pressures.

The model depends on two sets of empirical data to make these predictions: **strain-controlled LCF data** from axial coupons[2] (which produces strain-life and cyclic stress strain curves) and **constant pressure CT fatigue data**, generated on specialized coiled tubing testing fixtures that cycle tubing over curved and straight bending mandrels until failure at a constant internal pressure.

At the time the V3 was initially developed, material parameters only existed for four coiled tubing materials: Quality Tubing grades QT-700, QT-800 and QT-1000, and Precision Tubing grade HS-90. Since that time, material parameters were also developed for HS-110, QT-900 and QT-1200. During the generation and regression of the strain-controlled LCF parameters, it became apparent that the previous approach used to fit curves through LCF data was not the most appropriate approach. The curves were used to do the best job fitting the data over their experimental range, but the curves did not make reasonable extrapolations to the higher cycle life regime (e.g., lives associated with low pressures and large bending radius). Attempts to extrapolate the use of the model into the high cycle regime, beyond its experimentally validated range, were not reasonable. This brought to light some fundamental differences between the LCF coupon data and the low-pressure fixture data. The strain state caused by low-pressure fixture cycling in the wall of a CT sample is very similar to the dynamic strain state in the gauge section of a constant amplitude strain-controlled axial coupon. However, the data from these tests simply do not correlate well in the low-pressure regime ***for some materials***. Since the development of the CT fatigue algorithm had focused more on the high-pressure regime, there was initially no empirical means to account for this lack of correlation.

In V4, all strain-controlled LCF data were re-regressed, and a more fundamental Manson-Coffin curve was used to fit the initiation and fracture data. Furthermore, an additional empirical parameter was introduced to improve correlation in the low-pressure regime. The standard "coiled tubing exponent" (the exponent, "C" in Equation 16 from Reference 1 was correspondingly adjusted over the high-pressure regime, such that V4 now shows improved correlation over all life regimes for all CT materials. Keep in mind that lack of low-pressure correlation in V3 was only apparent in a few of the 6 materials, and nonexistent in the others. The V4 approach makes more fundamentally reliable extrapolations into the higher cycle life regime (a common occurrence in real applications since gooseneck radii are often much larger than the bending radii on CT fatigue testing fixtures).

Specifically, the changes implemented in the V4 model are listed below:

1. The strain-controlled LCF axial coupon data were re-regressed for all materials. More fundamental Manson-Coffin curves were fit to all initiation and fracture data.

2. An additional empirical Tubing Factor (TF) parameter was introduced to improve correlation in the low-pressure, high-cycle regime.

3. A bug associated with purely elastic cycling was removed.

These changes are described in this report, followed by a comparison of predictions from V4 and V3 with experimental data for all materials.

Strain-Controlled LCF Parameter Regression

Strain controlled fatigue data are used to regress the Ramberg-Osgood cyclic stress-strain relation and the Manson-Coffin strain-life equation. These relations are presented below (Equations 7 and 18, respectively, in Reference 1).

$$\varepsilon_a = \frac{\sigma_a}{E'} + \left(\frac{\sigma_a}{K'}\right)^{\frac{1}{n'}} \qquad \text{EQ 1}$$

$$\varepsilon_{a,eff} = \frac{\sigma_f'}{E'}(2N)^b + \varepsilon_f'(2N)^c \qquad \text{EQ 2}$$

The parameters for these relations are presented in Table 1. Notice that both "initiation" and "fracture" parameters are listed in Table 1 for Equation 2. A notable difference between V4 and V3 is the fact that the fatigue strength and ductility exponents, *b* and *c* respectively, are the same for initiation and fracture curves, in each material. This is not a coincidence, but was done to circumvent a problem associated with simply using the "best fit" through initiation and fracture data. These exponents, *b* and *c*, represent the slope of the elastic and plastic strain-life lines on logarithmic coordinates. In V3, the slopes of the fracture curves were slightly steeper than those for the elastic curves. When extrapolating to very long lives (approximately a million or more) the lines cross unreasonably. Since the values for *b* and *c* were found to be very similar, the average value was taken for both, and the fatigue strength and ductility coefficients, σ_f' and ε_f' respectively, were adjusted accordingly to provide a least-squares fit to initiation and fracture data, thus avoiding the crossover problem.

TABLE 1 *Material LCF Properties*

Property	QT-700	QT-800	QT-900	QT-1000	QT-1200	HS-90	HS-110
$S_{y,nom}$ (ksi)	70	80	90	100	120	90	110
E (ksi)	22,910	22,513	25,487	23,318	24,963	24,297	24,242
K′ (ksi)	76.57	111.02	109.62	116.67	150.58	95.48	130.29
n′	0.06734	0.09537	0.08042	0.05326	0.070969	0.06227	0.07496
σ_f' (ksi)	148.77	140.19	155.24	199.32	241.50	174.74	187.37
b	-0.14305	-0.1064	-0.11755	-0.1268	-0.13275	-0.136	-0.12055
ε_f'	1.09019	0.78574	0.34656	0.82356	0.81532	1.04388	0.50013
c	-0.7566	-0.7549	-0.6429	-0.82135	-0.8782	-0.7914	-0.74995
σ_f' (ksi)	153.75	142.88	158.84	205.44	248.88	178.91	191.38
b	-0.14305	-0.1064	-0.11755	-0.1268	-0.13275	-0.136	-0.12055
ε_f'	1.30490	0.90567	0.39288	1.00178	0.99484	1.19754	0.57065
c	-0.7566	-0.7549	-0.6429	-0.82135	-0.8782	-0.7914	-0.74995
TF	1.94	1.16	1.26	1.46	1.05	1.12	0.95

All seven sets were closely analyzed during the regression process to obtain the parameters presented in Table 1. For purposes of illustration, strain-life curves are shown for QT-1000 in Figure 1. This figure shows curves for total, elastic and plastic strain amplitude versus life to initiation and fracture. Strain amplitude data are also shown for all strain components versus life to initiation, and total strain data versus life to fracture. The cyclic stress-strain curves for all CT materials are shown in Figure 2, along with all stress versus total strain data points for all materials.

Figure 3 shows the strain-life (to fracture) curves for all CT materials. These curves display a typical trend - lower lives for higher strength materials with increasing strain range, and longer lives for higher strength materials with decreasing strain range, with some exceptions in the higher cycle regime where no data exist. When shown with the actual life to fracture data points in Figure 4, the importance of fundamentally valid curves for extrapolating into the high cycle regime is illustrated. Data are only generated for lives out to a few thousand cycles. Some experimental difficulties must be overcome to generate valid CT axial coupon data in the higher cycle regime (lives beyond 10^5 - 10^6 cycle range).

Low Pressure Empirical Parameter

Table 1 contains a new empirical "tubing factor," TF. In general, strain-controlled axial fatigue data for all materials (except HS-110) exhibit slightly longer lives than do coiled tubing samples, cycled with low internal pressure at the same strain range. There are several possible explanations for this (the strain gradient through the surface of the tubing, the presence of the pressurized fluid at the inner surface of the tubing, the presence of the internal weld flash on the tubing samples, etc.) although a thorough investigation has not been conducted. In order to address this discrepancy, an empirically determined life reduction factor, TF, was determined by trial and error in order to shift the entire strain-life curve into agreement with low pressure coiled tubing data. This factor is applied during the regression of the coiled tubing exponent (the exponent, "C" in Equation 16 from Reference 1), which enhances correlation over the entire experimental pressure range.

The improved correlation afforded by this approach is apparent in the last chapter of this document. From Table 1, the biggest differences were found in the QT-1000 and QT-700 materials. The V3 life to fracture predictions in the low-pressure regime were predominantly non-conservative for these materials, while V4 predictions are significantly improved.

Elastic Bug Removal

When bending strains are decreased (by decreasing the tubing diameter and/or increasing the bending radius) to the point where the maximum bending stress does not exceed the cyclic yield strength of the material, then straining becomes completely elastic. Although this almost never occurs in an actual CT application, the model could be used to make predictions for extremely large spool - small tubing diameter combinations. Studies such as this revealed unexpected anomalous behavior as loading was decreased into the elastic regime. This turned out to be a minor bug in the coding (use of a "< or =" sign, as opposed to an "=" sign) that

simply never emerged for inelastic CT loading. The new code was stress tested using an algorithm that subjected it to a decreasing strain range resulting in smooth, reasonable life estimates into the millions of cycles.

Percent Extrapolation Factors

There are two major factors that contribute to the "loading" on a section of CT whenever an "event" (bending or straightening) occurs:

1. The change in bending strain caused by wrapping or unwrapping over a particular radius of curvature, R, during the event, and

2. the internal pressure, P.

The empirical parameters used by the TFATIGUE algorithm are based on constant pressure data generated at various locations (the tubing manufacturers or the University of Tulsa Fatigue Laboratory). However, only a finite number of data points exist for any particular material grade. These range in diameter, D, from 1.25" to 3.5", in wall thickness, *t*, from 0.078" to 0.204" and are tested on a bending radius, R, of either a 48" or 72", at pressures ranging from near zero to 15,000 psi. For a given combination of these parameters, the average bending strain range through the wall thickness is computed by

$$\Delta\varepsilon_x = \frac{(D-t)}{2R} \qquad \textbf{EQ 3}$$

and the average hoop stress by

$$\sigma_h = \frac{P\left(\frac{D}{t}-2\right)}{2} \qquad \textbf{EQ 4}$$

For each set of data, the range of $\Delta\varepsilon_x$ and σh (normalized by the nominal yield stress of the material, S_y) were plotted and used to define a trapezoidal range of data collection, as illustrated in Figure 5 and Figure 6 for QT-900 and QT-1000, respectively. If a particular loading combination lies in this region, the extrapolation factor is zero (no extrapolation is needed). If a point lies ***outside this region***, the percent extrapolation factors are computed for the Radius (PEFR) and Pressure (PEFT) as follows.

PEFR = Percent Extrapolation Factor Radius =

$$PEFR = \begin{cases} \dfrac{\left((\Delta\varepsilon_x)-(\Delta\varepsilon_x)_{max}\right)}{\left((\Delta\varepsilon_x)_{max}-(\Delta\varepsilon_x)_{min}\right)}(100\%) \text{ for } (\Delta\varepsilon_x) > (\Delta\varepsilon_x)_{max} \\ \text{or} \\ \dfrac{\left((\Delta\varepsilon_x)-(\Delta\varepsilon_x)_{min}\right)}{\left((\Delta\varepsilon_x)_{max}-(\Delta\varepsilon_x)_{min}\right)}(100\%) \text{ for } (\Delta\varepsilon_x) < (\Delta\varepsilon_x)_{min} \end{cases}$$

PEFP = Percent Extrapolation Factor Pressure is computed by:

$$PEFR = \begin{cases} \dfrac{(\sigma_h/S_y)-(\sigma_h/S_y)_{max}}{(\sigma_h/S_y)_{max}}(100\%) \text{ for } (\Delta\varepsilon_x) > (\Delta\varepsilon_x)_{max} \\ \text{or} \\ \dfrac{(\sigma_h/S_y)-(\sigma_h/S_y)_{min}}{(\sigma_h/S_y)_{min}}(100\%) \text{ for } (\Delta\varepsilon_x) < (\Delta\varepsilon_x)_{min} \\ \text{or} \\ \dfrac{(\sigma_h/S_y)-(\sigma_h/S_y)^*}{(\sigma_h/S_y)^*}(100\%) \text{ for } (\Delta\varepsilon_x)_{min} < (\Delta\varepsilon_x) < (\Delta\varepsilon_x)_{max} \\ \text{where} \\ (\sigma_h/S_y)^* = (\sigma_h/S_y)_{min} + \dfrac{(\sigma_h/S_y)_{max}-(\sigma_h/S_y)_{min}}{(\Delta\varepsilon_x)_{max}-(\Delta\varepsilon_x)_{min}}\left(\Delta\varepsilon_x-(\Delta\varepsilon_x)_{min}\right) \end{cases}$$

Therefore, the PEFP and PEFR parameters not only tell you the event lies outside the current experimental data range, but provide a quantitative measure about how far. Table 2 presents the bases for PEFP and PEFR calculations for all CT materials, to date, along with the total number of data points available for regression.

TABLE 2 *Bases for PEFT and PEFP Computations*

Material	# pts	ε_{max}	$(\sigma_h/S_y)_{min}$	ε_{max}	$(\sigma_h/S_y)_{max}$
QT-700	140	0.022986	0.672	0.011069	0.672
QT-800	552	0.017500	0.710	0.010600	0.500
QT-900	340	0.15563	0.786	0.011069	0.512
QT-1000	295	0.016927	0.500	0.011069	0.702
QT-1200	243	0.014229	0.500	0.011396	0.376
HS-90	240	0.023115	0.388	0.010938	0.500
HS-110	122	0.014229	0.786	0.010833	0.350

Comparison of Life Predictions from V4 and V3

Figures 5 through 20 are plots of experimental life on the y-axis versus estimated life on the x-axis using V4 and V3 for all coiled tubing samples. A line of perfect correlation is shown on each plot. Points lying above the line lasted longer than predicted (conservative predictions) and points lying below the line failed sooner than predicted (non-conservative predictions).

The largest difference between the two versions occurs with the QT-700 and QT-1000 materials, where the largest value of TF was required to correlate the low-pressure data. In these materials, (Figures 8 and 14), the accuracy of the predictions was improved considerably in the low-pressure (high cycle) regime. V3 predictions in both of these figures are predominantly non-conservative in the low-pressure regime. The TF parameter was less successful in correlating the HS-90 predictions across the entire pressure range. If the factor was adjusted to pull the low pressure predictions into good correlation, the higher pressure predictions became non-conservative.

Overall, improved correlation is provided by V4 relative to V3 in all materials.

Figures

FIGURE 1 Strain-Life initiation data (and total strain Fracture data) along with Manson- Coffin initiation and Fracture curves for QT-1000 material

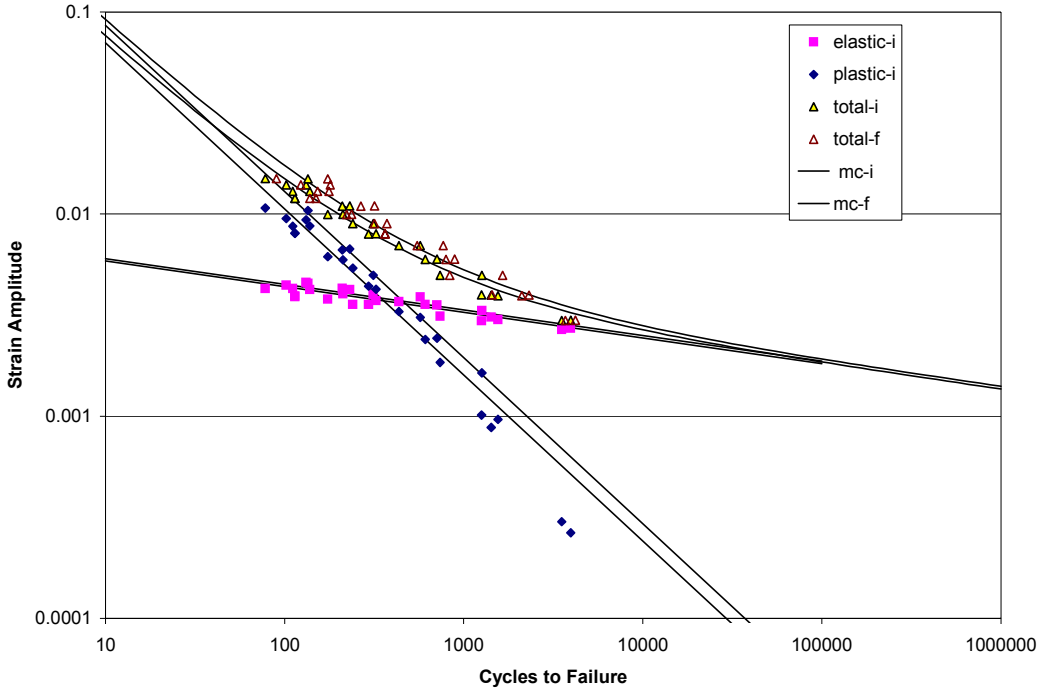

FIGURE 2 Cyclic stress-strain amplitude curves (Ramberg-Osgood) and data for all CT materials.

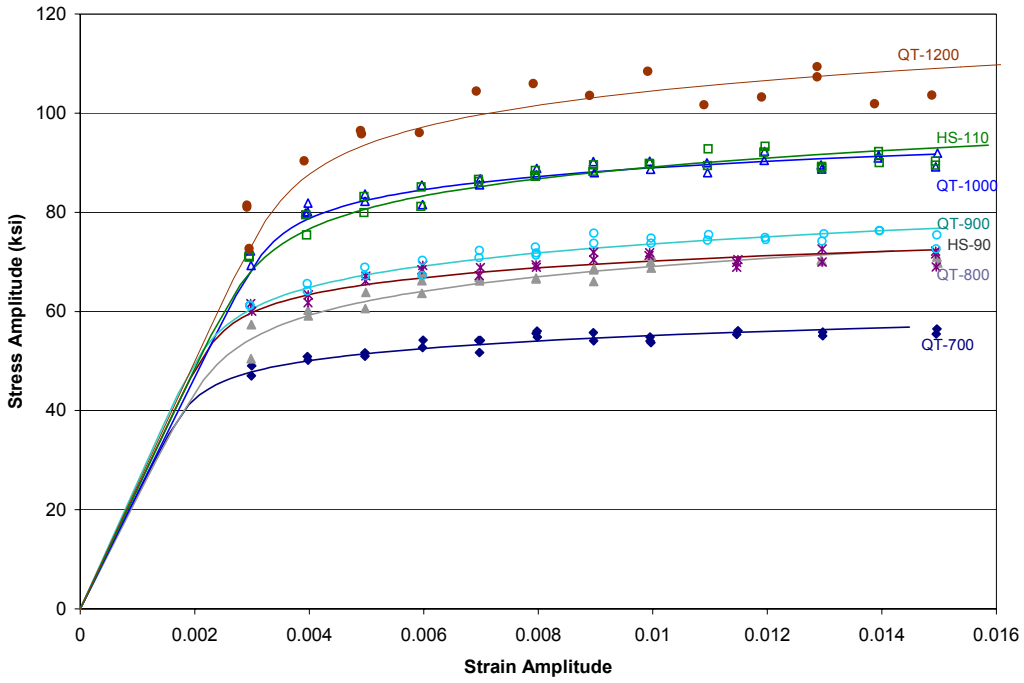

FIGURE 3 Strain-Life curves (Manson-Coffin) for all CT materials, based on cycles to Fracture.

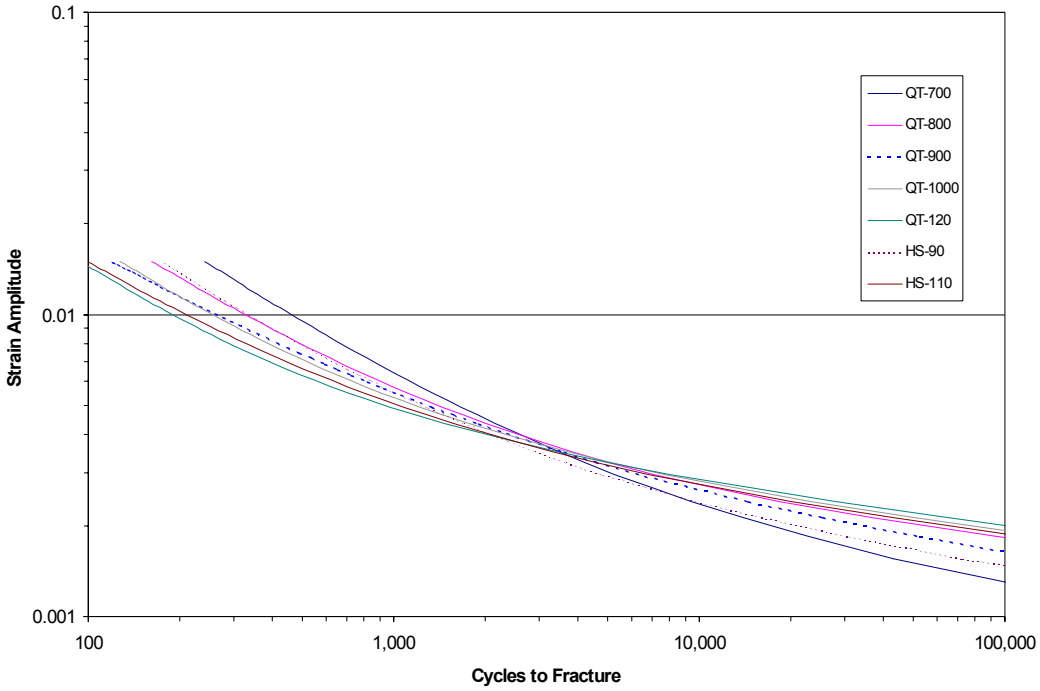

FIGURE 4 Strain-Life to Fracture curves (Manson-Coffin) for all CT materials, along with coupon data. Extrapolations are required for lives beyond a few thousand.

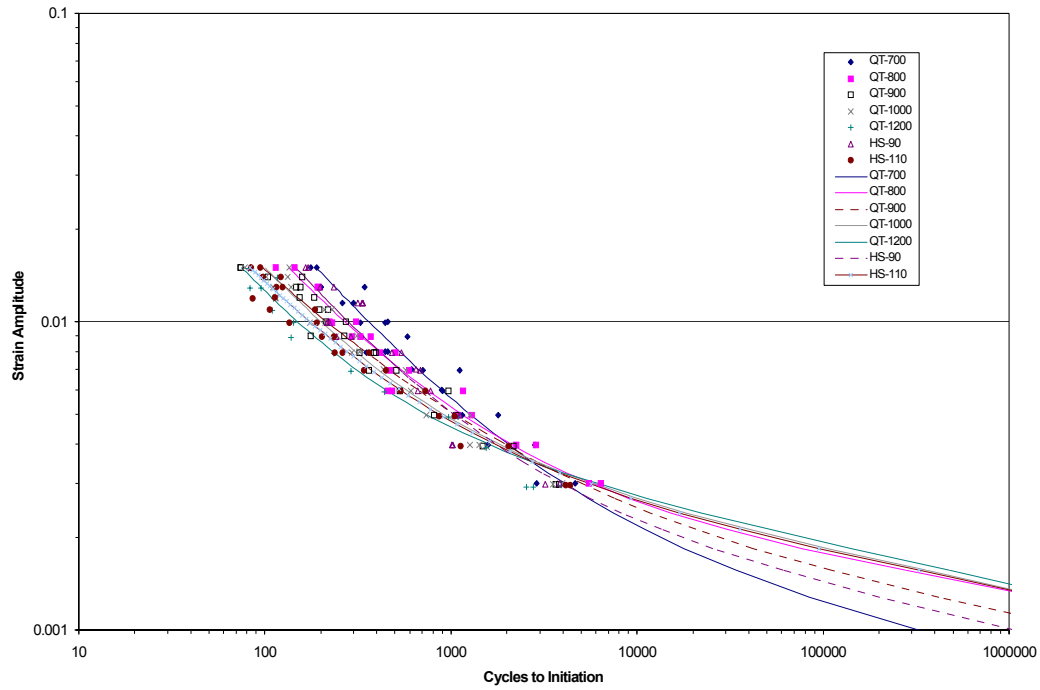

FIGURE 5 Illustration of PEFP and PEFR range for QT-900

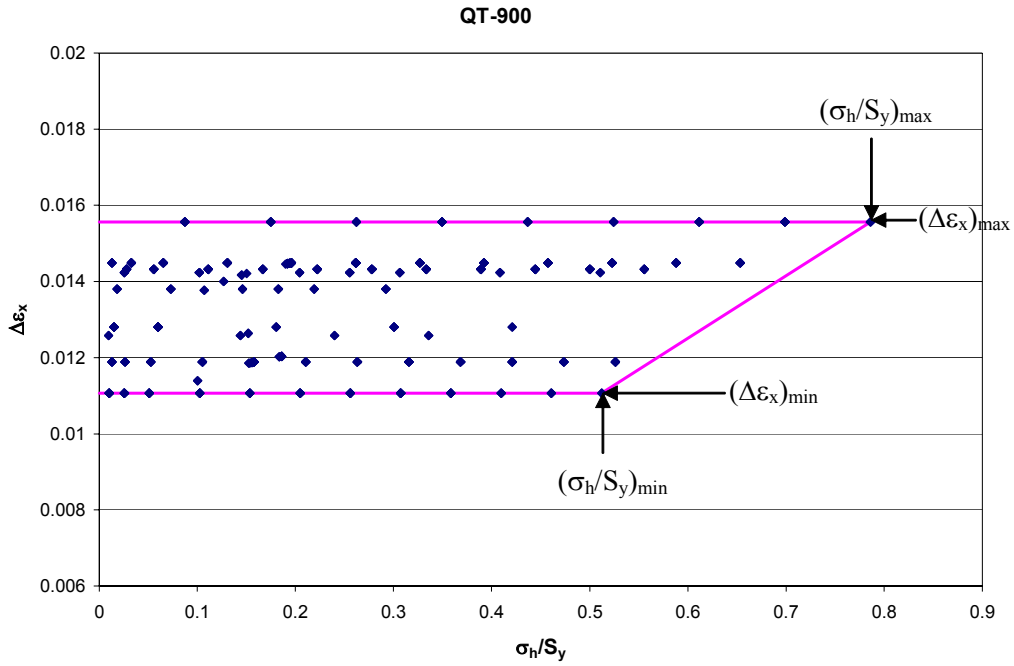

FIGURE 6 Illustration of PEFP and PEFR range for QT-1000

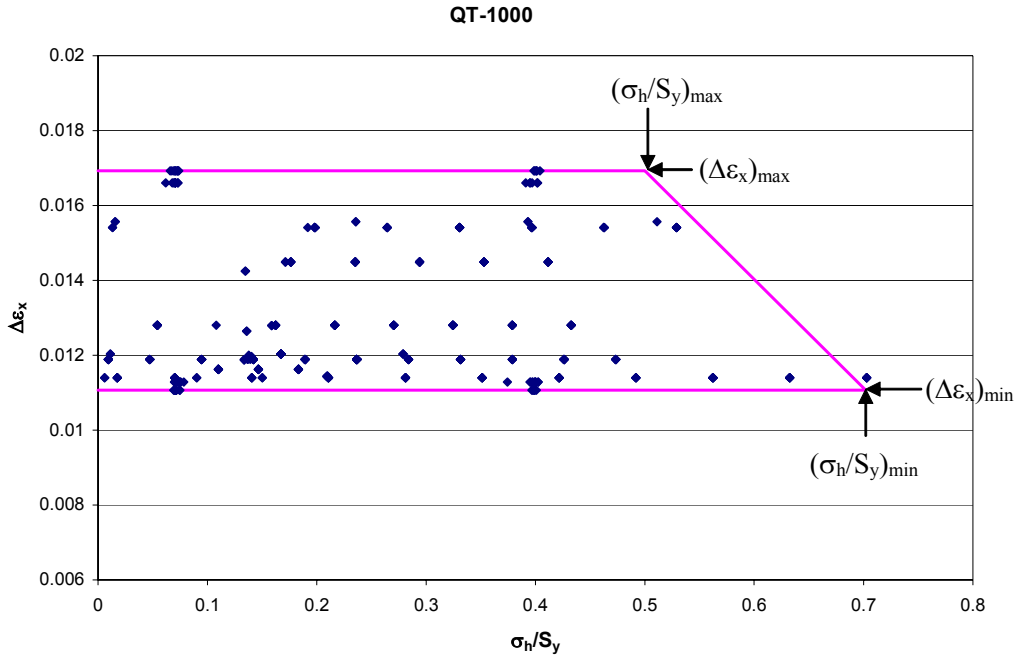

FIGURE 7 Experimental versus Predicted Life to Crack Initiation for QT-700

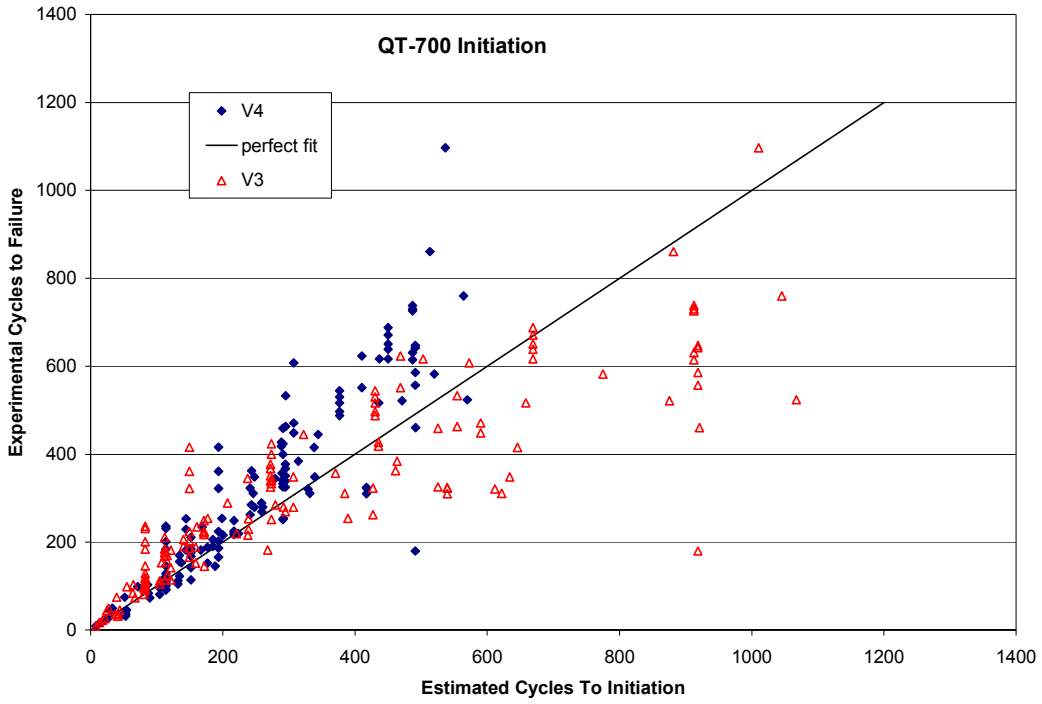

FIGURE 8 Experimental versus Predicted Life to Fracture for QT-700

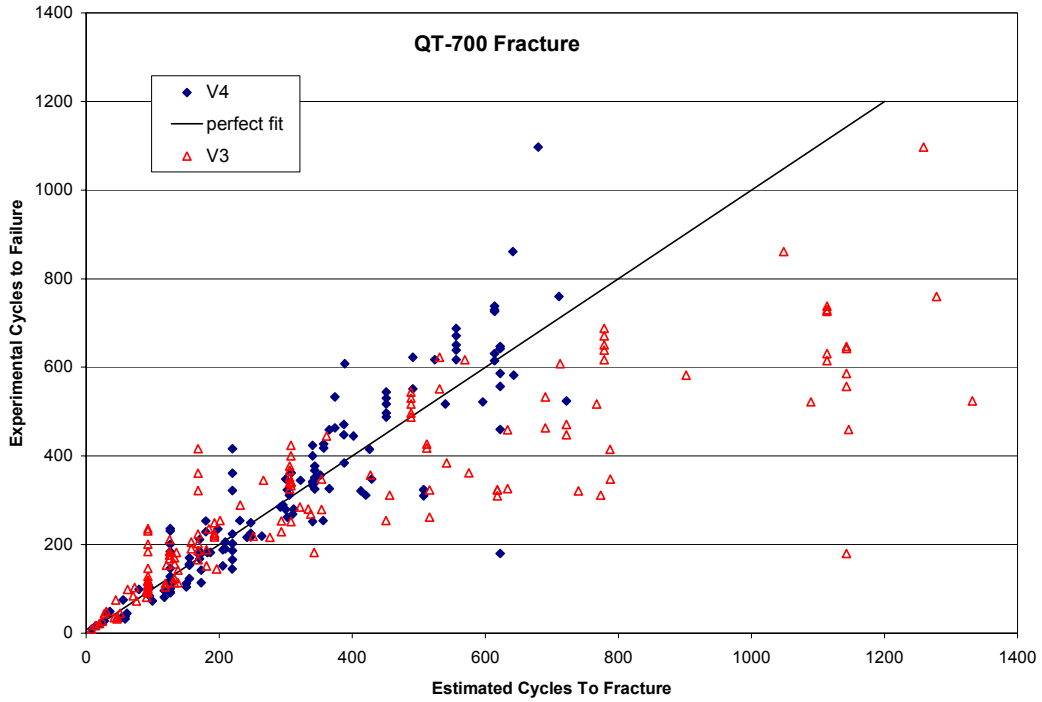

FIGURE 9 Experimental versus Predicted Life to Crack Initiation for QT-800

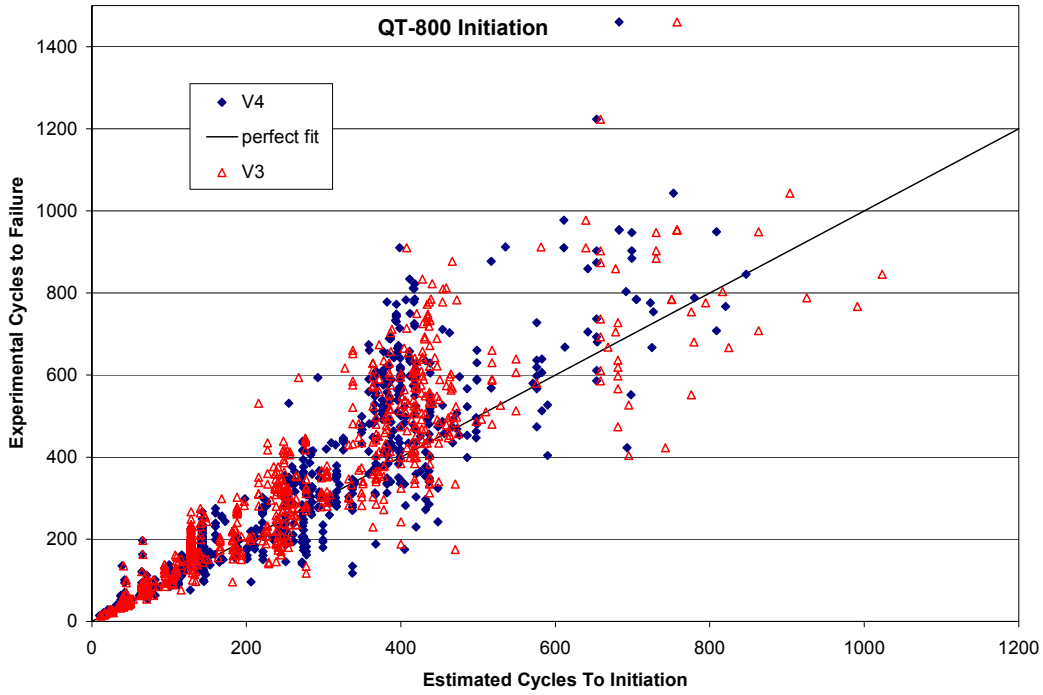

FIGURE 10 Experimental versus Predicted Life to Fracture for QT-800

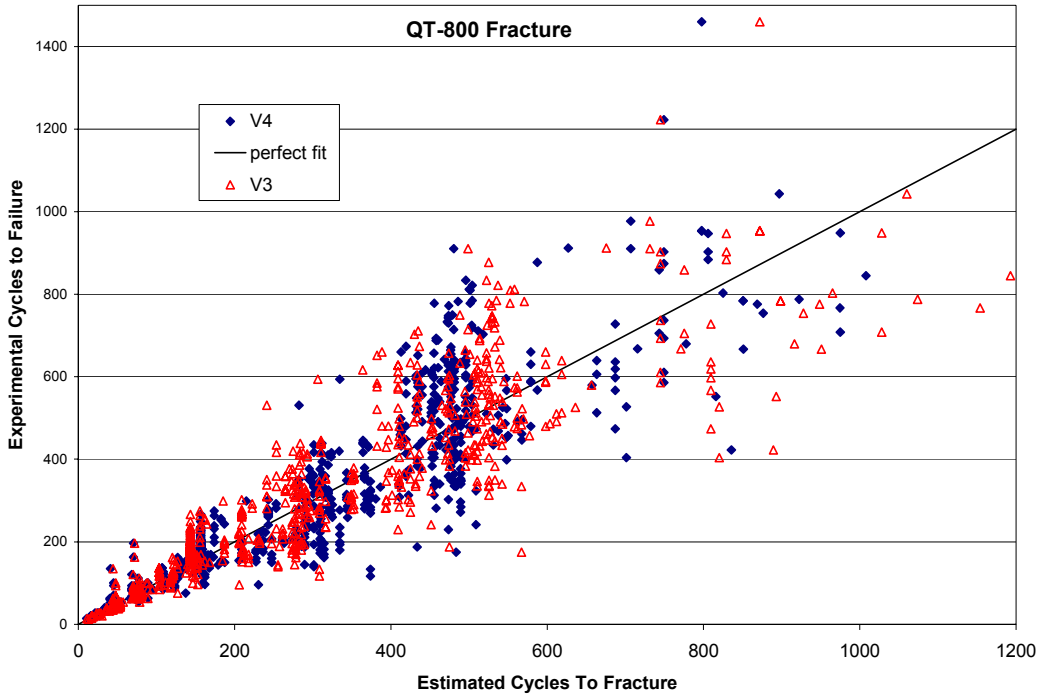

FIGURE 11 Experimental versus Predicted Life to Crack Initiation for QT-900

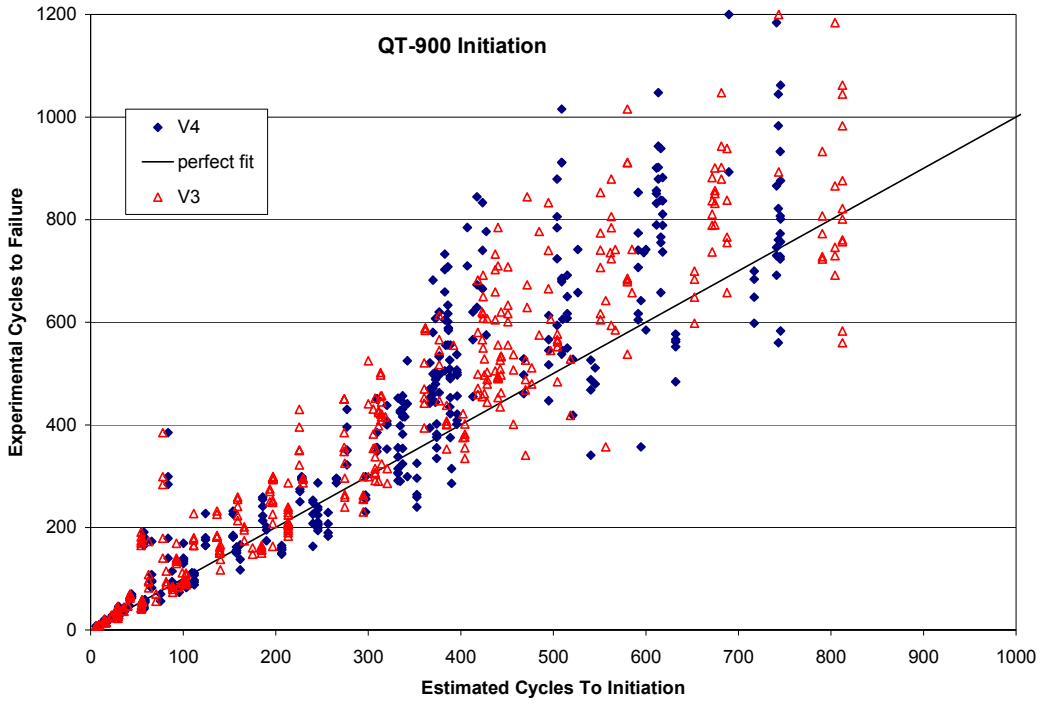

FIGURE 12 Experimental versus Predicted Life to Fracture for QT-900

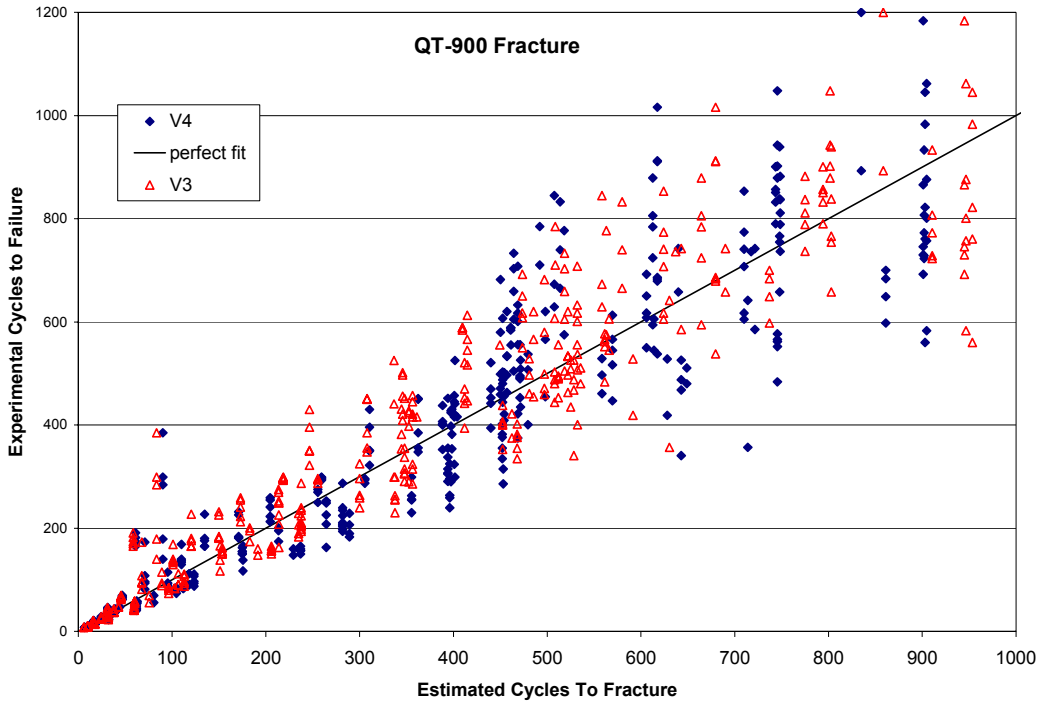

FIGURE 13 Experimental versus Predicted Life to Crack Initiation for QT-1000

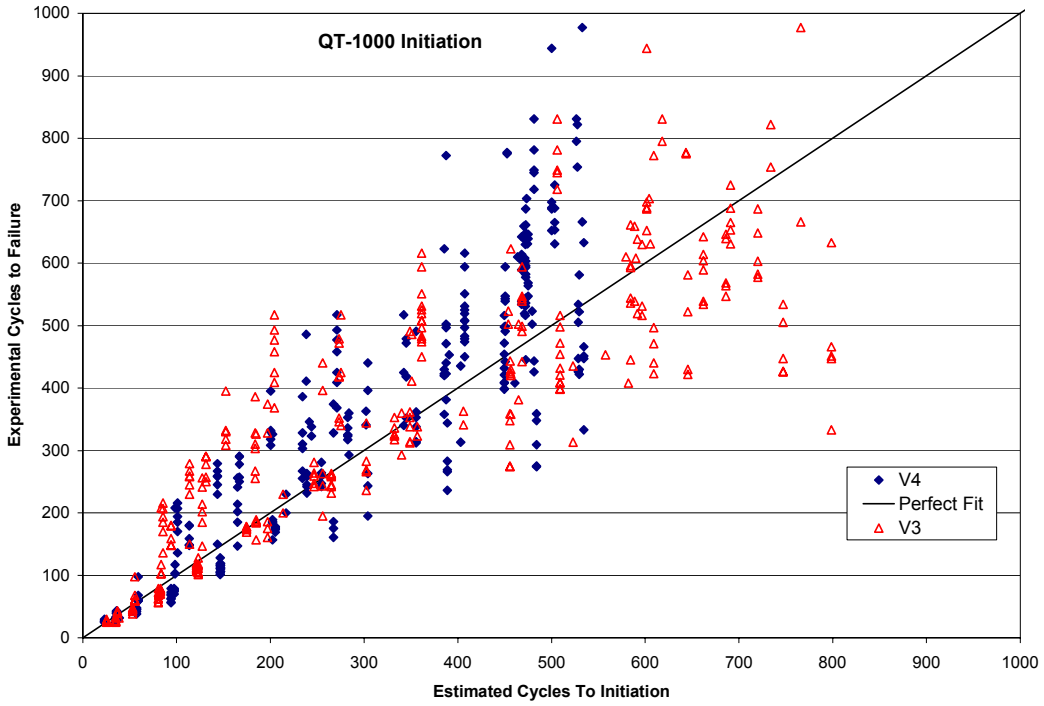

FIGURE 14 Experimental versus Predicted Life to Fracture for QT-1000

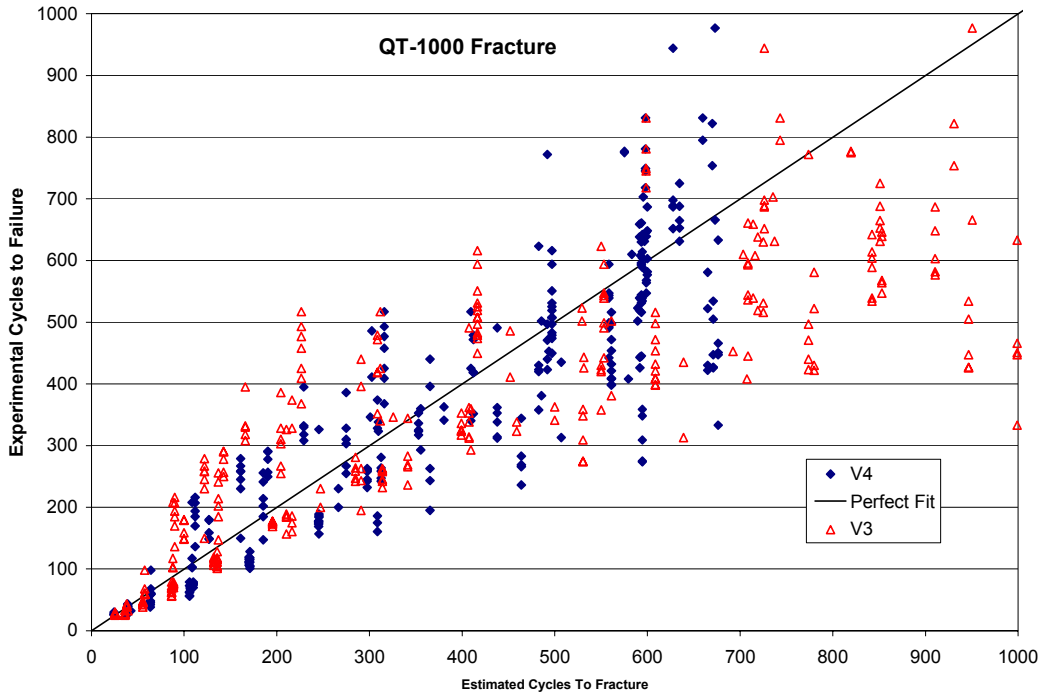

FIGURE 15 Experimental versus Predicted Life to Crack Initiation for QT-1200

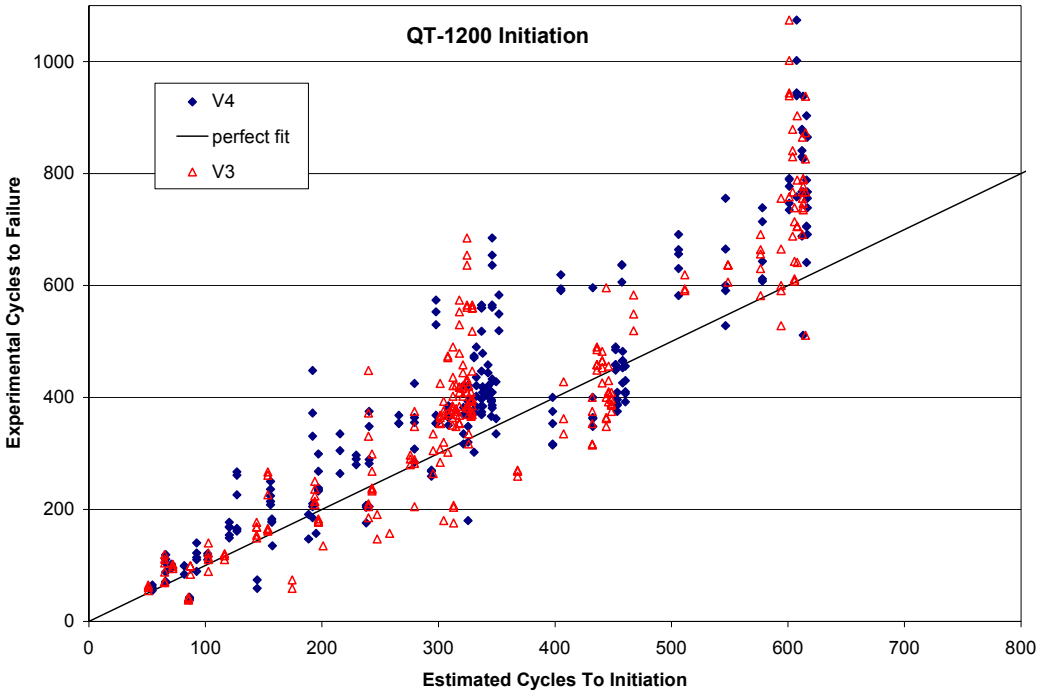

FIGURE 16 Experimental versus Predicted Life to Fracture for QT-1200

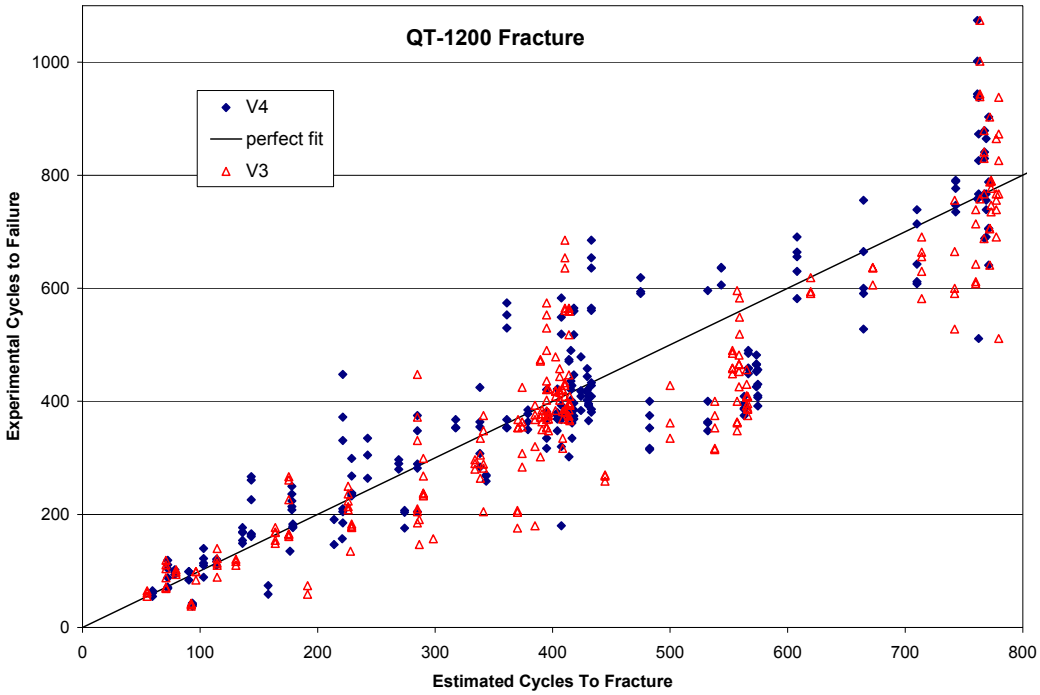

FIGURE 17 Experimental versus Predicted Life to Crack Initiation for HS-90

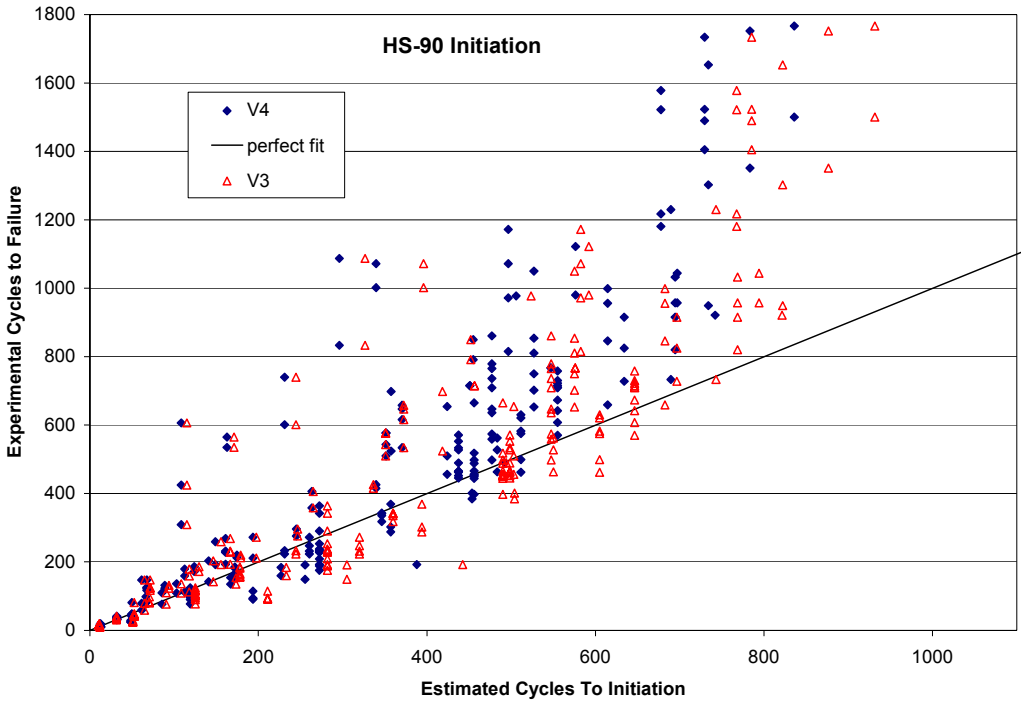

FIGURE 18 Experimental versus Predicted Life to Fracture for HS-90

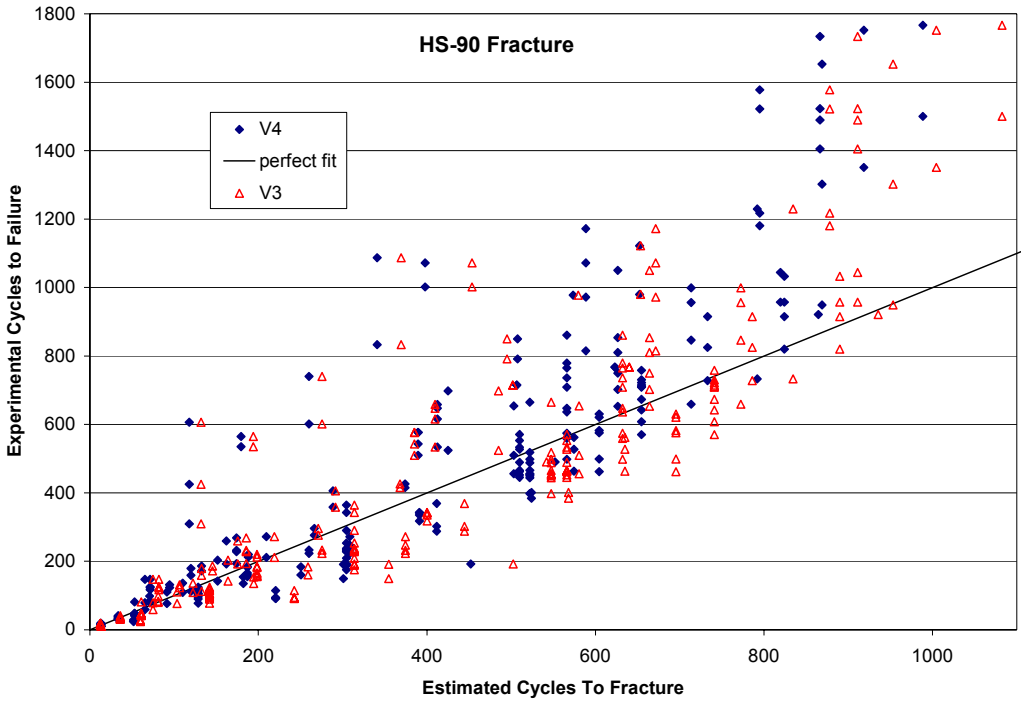

FIGURE 19 Experimental versus Predicted Life to Crack Initiation for HS-110

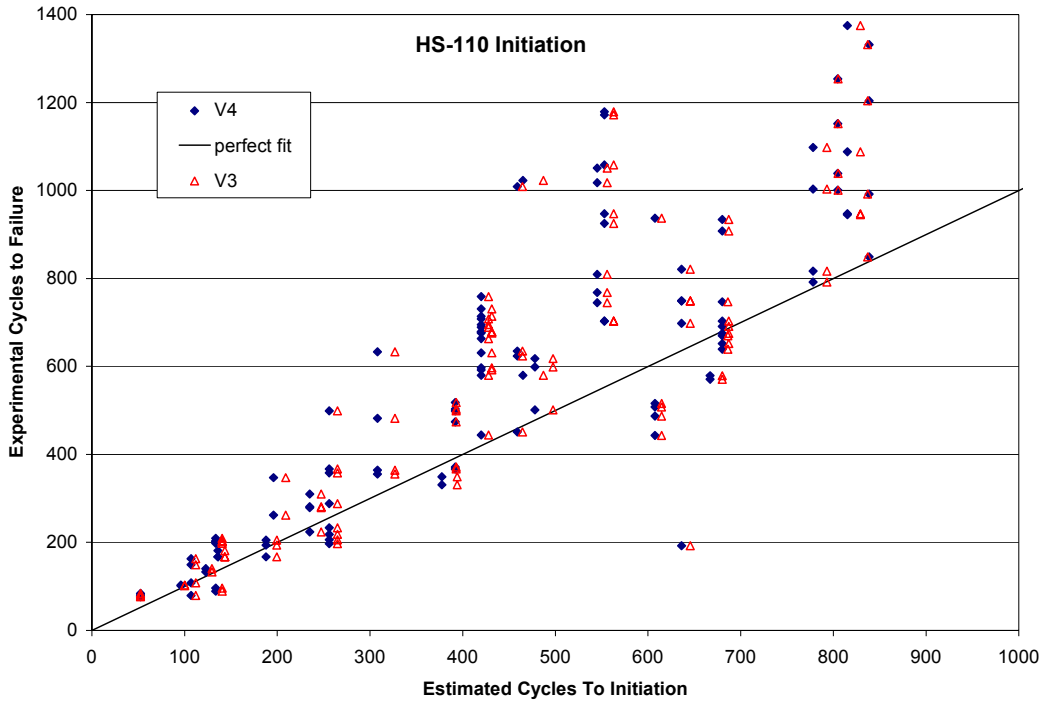

FIGURE 20 Experimental versus Predicted Life to Fracture for HS-110

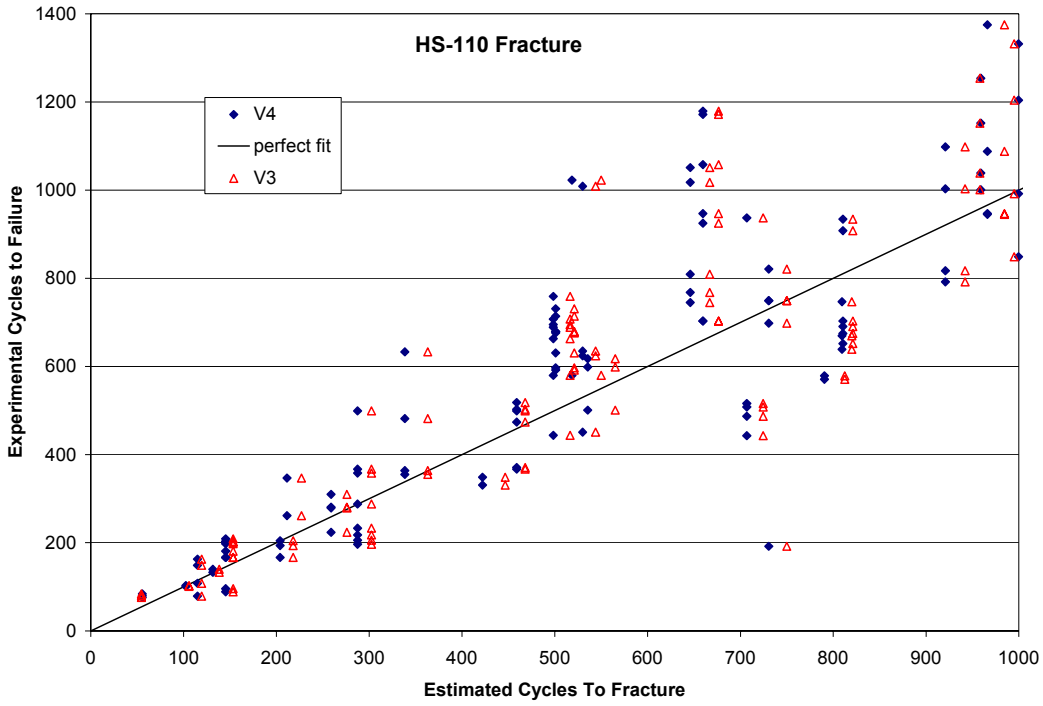

References

1. Tipton, S.M., "The Achilles Fatigue Model," CTES Tech Note, May, 1999.

2. Tipton, S.M., "Low-Cycle Fatigue Testing of Tubular Material using Non-Standard Specimens," Effects of Product Quality and Design Criteria on Structural Integrity, ASTM STP 1337, R. C. Rice and D. E. Tritsch, Eds., American Society for Testing and Materials, 1998.

CTES